

Spectral photon-number distribution of parametric down-conversion and generation of heralded Fock states

Yan-Sheng Bao(包燕升), Bo-Chen Wang(王搏尘), Chang-Yong Tian(田昌勇), Zheng-Yong Li(李政勇)
Citation: Chin. Phys. B, 2025, 34 (**7**): 074214. DOI: 10.1088/1674-1056/add904
http://cpb.iphy.ac.cn; http://iopscience.iop.org/cpb

What follows is a list of articles you may be interested in

Engineering the spectra of photon triplets generated from micro/nanofiber

Chuan Qu(瞿川), Dongqin Guo(郭东琴), Xiaoxiao Li(李笑笑), Zhenqi Liu(刘振旗), Yi Zhao(赵义), Shenghai Zhang(张胜海), and Zhengtong Wei(卫正统)
Chin. Phys. B, 2024, 33 (**3**): 034208. DOI: 10.1088/1674-1056/ad1c5d

Tunable phonon-atom interaction in a hybrid optomechanical system

Yao Li(李耀), Chuang Li(李闯), Jiandong Zhang(张建东), Ying Dong(董莹), and Huizhu Hu(胡慧珠)
Chin. Phys. B, 2023, 32 (**4**): 044213. DOI: 10.1088/1674-1056/acb9ea

Speeding up generation of photon Fock state in a superconducting circuit via counterdiabatic driving

Xin-Ping Dong(董新平), Xiao-Jing Lu(路晓静), Ming Li(李明), Zheng-Yin Zhao(赵正印), and Zhi-Bo Feng(冯志波)
Chin. Phys. B, 2021, 30 (**4**): 044214. DOI: 10.1088/1674-1056/abe297

A scheme for Sagnac-effect quantum enhancement with Fock state light input

Kun Chen(陈坤), Shu-Xin Chen(陈树新), De-Wei Wu(吴德伟), Chun-Yan Yang(杨春燕), Qiang Miao(苗强)
Chin. Phys. B, 2017, 26 (**9**): 094212. DOI: 10.1088/1674-1056/26/9/094212

Quantum interference between heralded single photon stateand coherent state

Lei Yang(杨磊), Xiaoxin Ma(马晓欣), Xiaoying Li(李小英)
Chin. Phys. B, 2017, 26 (**7**): 074206. DOI: 10.1088/1674-1056/26/7/074206

Spectral photon-number distribution of parametric down-conversion and generation of heralded Fock states

Yan-Sheng Bao(包燕升)[1,2], Bo-Chen Wang(王搏尘)[1,2], Chang-Yong Tian(田昌勇)[3,†], and Zheng-Yong Li(李政勇)[1,2,‡]

[1] *Department of Physics, Beijing Jiaotong University, Beijing* 100044, *China*
[2] *Key Laboratory of Education Ministry on Luminescence and Optical Information Technology, Beijing Jiaotong University, Beijing* 100044, *China*
[3] *Technical Institute of Physics and Chemistry, Chinese Academy of Sciences, Beijing* 100190, *China*

(Received 3 March 2025; revised manuscript received 4 May 2025; accepted manuscript online 15 May 2025)

Photon pairs with large nondegeneracy have recently attracted increasing interest, which gives rise to an urgent demand for revealing their complete and accurate spectral distribution. By thoroughly analyzing parametric down-conversion (PDC), we put forward a model to directly describe the spatial-spectral distribution of these photon pairs, which is experimentally demonstrated by a 532-nm pumped type-I PDC in a beta barium borate (BBO) crystal. The measured spectral curves show good agreement with the theoretical predictions over the entire spectral range. We further demonstrate that, as signal wavelength increases, the photon pairs are initially spectrally distinguishable, then partly indistinguishable, finally completely indistinguishable with a maximum bandwidth of approximately 500 nm. Utilizing photon-number-resolving single-photon detectors (SPD), we observe the average photon number decreases significantly more slowly than the spectral intensity as the wavelength deviates from the peak, and the photon numbers follow a quasi-Poisson distribution well for wavelengths around the peak, but a thermal distribution better describes the statistics near the spectral boundaries. Finally, we use the signal photons as the trigger to generate heralded Fock states up to 10 photons in near-infrared range, which are suitable for quantum simulation and quantum key distribution in optical fiber networks.

Keywords: photon-number distribution, parametric down-conversion, Fock state

PACS: 42.50.–p, 03.67.–a, 42.65.Lm

DOI: 10.1088/1674-1056/add904 **CSTR:** 32038.14.CPB.add904

1. Introduction

Parametric down-conversion (PDC) plays an important role in promoting novel quantum technologies and their applications,[1] such as the generation and distillation of squeezed states,[2–5] a polarization-entangled photon source for quantum communication and imaging,[6–10] momentum-position entangled photons that significantly improve image contrast,[11] and entanglement-enhanced interferometers based on quantum computing logic unit.[12] To produce high-quality photon pairs for advanced applications,[13–17] it is indeed necessary to completely investigate their spectral properties.

During the last two decades, a number of reports have been published on various PDC cases. For example, Grice *et al.*[18] obtained the joint spectral intensity of degenerate type-II down-conversion in beta barium borate (BBO), Kim and Grice[19] measured the spectral properties of the two-photon state generated via type-II PDC, Jin *et al.*[20] generated spectrally uncorrelated biphoton states, and Kuzucu *et al.*[21] performed joint temporal density measurements for the two-photon state produced by ultrafast type-II PDC using time-resolved single-photon detection.

In recent years, nondegenerate PDC, especially with wide nondegeneration, has been attracting increasing interest. For instance, nondegenerate broadband photon pairs have been used to implement near-infrared quantum spectrophotometers,[13,16] quantum-optical coherence tomography,[14] quantum imaging with undetected photons,[15,22] among other applications. These advances motivate us to conduct a thoroughgoing investigation of their spectral characteristics and hidden facets. We focus on the spectral photon-number distribution of widely nondegenerate photon pairs using photon-number-resolving detection.

2. Principle

The spectral distribution is mainly determined by the phase-matching conditions in a nonlinear medium. Considering PDC multimode squeezing[23] in nonlinear crystal BBO as shown in Fig. 1(a), the phase mismatch (Δ) will cause bandwidth broadening of PDC photons, which can be expressed by[19,24]

$$\Delta\left(\lambda_{\mathrm{s}},\lambda_{\mathrm{i}},\theta_{\mathrm{s}}'\right) = k_{\mathrm{p}}\left(\lambda_{\mathrm{p}},\Psi\right) - k_{\mathrm{s}}\left(\lambda_{\mathrm{s}}\right)\sqrt{1-\left(\sin\theta_{\mathrm{s}}'/n_{\mathrm{o}}\left(\lambda_{\mathrm{s}}\right)\right)^2} - k_{\mathrm{i}}\left(\lambda_{\mathrm{i}}\right)\sqrt{1-\left(\lambda_{\mathrm{i}}\sin\theta_{\mathrm{s}}'/\lambda_{\mathrm{s}}n_{\mathrm{o}}\left(\lambda_{\mathrm{s}}\right)\right)^2}, \quad (1)$$

†Corresponding author. E-mail: tcy@mail.ipc.ac.cn
‡Corresponding author. E-mail: zhyli@bjtu.edu.cn

© 2025 Chinese Physical Society and IOP Publishing Ltd. All rights, including for text and data mining, AI training, and similar technologies, are reserved.

where λ_j and k_j (j = p, s, i) are the wavelength and wave vector of the pump, signal, and idler photons, θ_s' and θ_i' are outside angles of signal and idler photons, and Ψ is the inner angle between the pump and optical axis. Then the joint spectral probability distribution can be calculated by[18,19]

$$S(\lambda_s, \lambda_i) = \mathrm{sinc}^2\left(\frac{\Delta\lambda_s\theta_s' L}{2}\right) \mathrm{e}^{-\frac{(\omega_s+\omega_i-\Omega_p)^2}{\sigma_p^2}}, \tag{2}$$

where σ_p is the linewidth of the pump laser, L is the length of the nonlinear crystal, Δ is the phase mismatch, ω_s and ω_i are frequencies of signal and idler photons, and Ω_p is the central frequency of the pump laser.

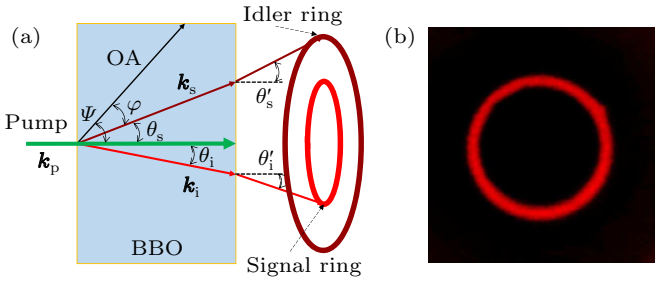


Fig. 1. (a) PDC phase matching (OA: optical axis). (b) Signal ring image of PDC photons.

Generally, we can obtain the spectral distribution of signal or idler photons only by numerical calculation according to Eqs. (1) and (2). However, considering most cases of PDC pumped by a narrow-linewidth laser, we can derive an analytic expression to describe the marginal spectral distribution of photon pairs as

$$S(\lambda_s, \Psi) = \xi_p \,\mathrm{sinc}^2(\pi L) \times \left[\frac{\delta n_{is}}{\lambda_s} + \frac{\delta n_{pi}}{\lambda_p} + \frac{\sin^2\theta_s'(\lambda_s n_o(\lambda_s) + \lambda_p \delta n_{is})}{2\lambda_s(\lambda_s - \lambda_p) n_o^2(\lambda_s)}\right]. \tag{3}$$

Here, $\delta n_{is} = n_o(\lambda_i) - n_o(\lambda_s)$, $\delta n_{pi} = n_{eff}(\lambda_p, \Psi) - n_o(\lambda_i)$, n_{eff} denotes the effective refractive index, and $\xi_p = 1 - (\omega_p - \Omega_p)^2/\sigma_p^2$ describes the effect due to pump laser linewidth. To obtain the spectral distribution of idler photons, we just need to simply exchange the two subscripts "s" and "i" in Eq. (3).

When the pump is quasi-monochromatic, PDC photons obey the thermal distribution approximately. However, practical pump lasers have certain bandwidths; together with limited acquisition speed of single-photon detectors (SPD), counted photons are usually in different modes, especially under a strong pump, which results in a multi-mode distribution.[23] In this case, the probability distribution of n photons is given by[25]

$$P(n) = \frac{(n+m-1)!}{n!(m-1)!\left(1+\frac{\langle n\rangle}{m}\right)^n\left(1+\frac{m}{\langle n\rangle}\right)^m}, \tag{4}$$

where m is the number of temporal modes and $\langle n\rangle$ is the mean photon number.

According to Eqs. (3) and (4), the spectral distribution of photon pairs exhibits a peak counting rate in the middle of their spectrum, while it gradually decreases and reaches a minimum at both ends. Thus, for a practical PDC system with a narrow-linewidth pump, due to weak photon generation at the spectral edges, the SPD can register a single temporal mode with one click so that the PDC photons agree well with the thermal distribution. When the wavelength approaches the peak, the PDC becomes stronger and stronger, and the SPD will count different temporal modes, leading to a multi-thermal distribution. At the peak wavelength, the PDC is so powerful that its photons follow a distribution close to a quasi-Poisson distribution.

3. Spectral photon-number distribution measurement

To prove their validity, we establish the experimental setup shown in Fig. 2. First of all, we carefully select a narrow-linewidth continuous-wave (CW) pump laser (Nd:YVO_4, λ = 532 nm, $\sigma_p < 5$ MHz, Coherent Inc.), and employ a high-speed acousto-optic modulator (AOM) to generate a pulsed pump laser, whose trigger gates the detectors to reduce most of the dark counts. In order to obtain a pure 532-nm laser beam, in addition to a band-pass filter, we use a dispersion prism to further remove unwanted background fluorescence. With a rotatable half-wave plate (HWP) to adjust the polarization state, the pump laser is focused through a plano-convex lens (f = 300 mm) onto the β-BBO crystal ($5\times5\times1$ mm^3, $\theta = 19.8°$, $\varphi = 0°$, CASTECH Inc.) mounted on a rotation stage. By finely tuning the internal angle between the β-BBO crystal optical axis and the pump, we can change the center wavelengths of the output entangled photon pairs.

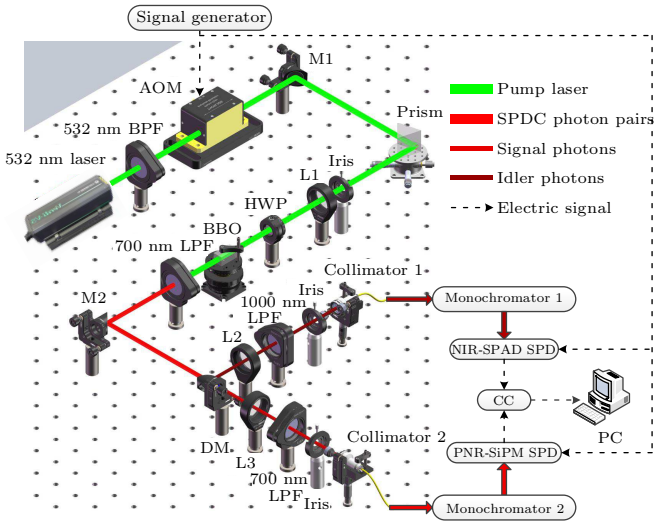


Fig. 2. Experimental configuration for measuring spectral photon-number distribution of entangled photons in widely nondegenerate PDC. (BPF: band-pass filter; M1 and M2: mirror; L1, L2, and L3: plano-convex lenses; LPF: long-pass filter; DM: dichroic mirror; CC: coincidence counting module; PC: personal computer).

After blocking the remnant pump light by a high-performance long-pass interference filter (FELH0700, Thorlabs Inc.), the photon pairs are separated using a dichroic mirror (short-pass, $\lambda_{\text{cutoff}} \sim 1000$ nm) into two parts (signal and idler), both of which are collimated by plano-convex lenses ($f = 200$ mm). Then the signal ($\lambda_s < 1000$ nm) and idler photons ($\lambda_i > 1000$ nm) first pass through an iris to ensure that the collected photons are collinear. Subsequently they are filtered by corresponding monochromators, then detected by a homemade photon-number-resolving (PNR) photomultiplier tube (PMT) (H7422P-50 Hamamatsu) and near-infrared avalanche photodiode (NIR-APD) SPDs, respectively. Scanning the transmission wavelength of the monochromators while recording the counts of two detectors in coincidence mode, we obtain the spectral distribution of photon pairs accurately.

According to our calculation, when the 1-mm β-BBO crystal is pumped by a 532-nm laser with $21.0^\circ < \Psi < 22.8^\circ$, nondegenerate PDC photons can be generated at the collinear position. When $\Psi = 22.8^\circ$, degenerate 1064-nm photons are emitted collinearly. For $\Psi \geq 23^\circ$, collinear PDC photons disappear completely, only non-collinear PDC photons can be observed. To verify this, we use an electron-multiplying charge-coupled device (EMCCD) camera to measure the PDC signal photons in this regime. For exposure time of 15 s, we obtain the image shown in Fig. 1(b), where one can see a clear hollow ring indicating that the probability of collinear PDC photons is too low to be observed compared with non-collinear ones.

Next we focus on the spectral distribution of widely nondegenerate PDC photons. Our analysis results show the PDC process is highly sensitive to angle Ψ, and a variation of just one tenth of a degree can produce very different spectral distribution. To demonstrate this, we consider two typical cases ($\Psi = 22.20^\circ, 22.45^\circ$) in the range of collinear phase matching. According to Eq. (3) we calculate the spatial distribution of the PDC photons and their joint spectrum. The results are illustrated in Fig. 3, from which we find that, for $\Psi = 22.20^\circ$ the peak wavelengths of the photon pairs are $\lambda_s = 820$ nm and $\lambda_i = 1515$ nm, while their bandwidths are $\Delta\lambda_s = 120$ nm and $\Delta\lambda_i = 370$ nm. However, when $\Psi = 22.45^\circ$, the peak wavelengths are $\lambda_s = 870$ nm and $\lambda_i = 1370$ nm, and their bandwidths are $\Delta\lambda_s \simeq 195$ nm and $\Delta\lambda_i \simeq 465$ nm, which differ significantly from the previous case although Ψ increases only 0.25°.

To achieve spectral distributions of signal and idler photons separately, we first calculate both of their spectral curves based on Eq. (3). The calculated results are plotted in Fig. 4 as dash lines, which are smooth curves with obvious peaks. Then we perform the measurements using the experimental setup in Fig. 2, where for the signal arm, the average dark counts are around 10 counts per second (cps); while for the idler arm, the NIR-APD has an average dark count of 500 cps. We record the counts of signal photons every 6 nm from 765 nm to 885 nm, and for the idler photons the counts are recorded every 10 nm from 1310 nm to 1660 nm, resulting in the spectral distribution curves as shown in Fig. 4 by solid lines. Experimental results show that, for $\Psi = 22.20^\circ$, the maximum signal counts are 340 cps around 825 nm and the measured bandwidth $\Delta\lambda_s \simeq 116$ nm, which are close to the theoretical values of 820 nm and 120 nm; for idler photons, the maximum count is 2200 cps at 1520 nm near the theoretical value of 1515 nm. Due to the spectral response curve of the NIR-APD, the measured bandwidth $\Delta\lambda_i \simeq 340$ nm is slightly lower than the theoretical value 370 nm. When $\Psi = 22.45^\circ$, the peak wavelengths

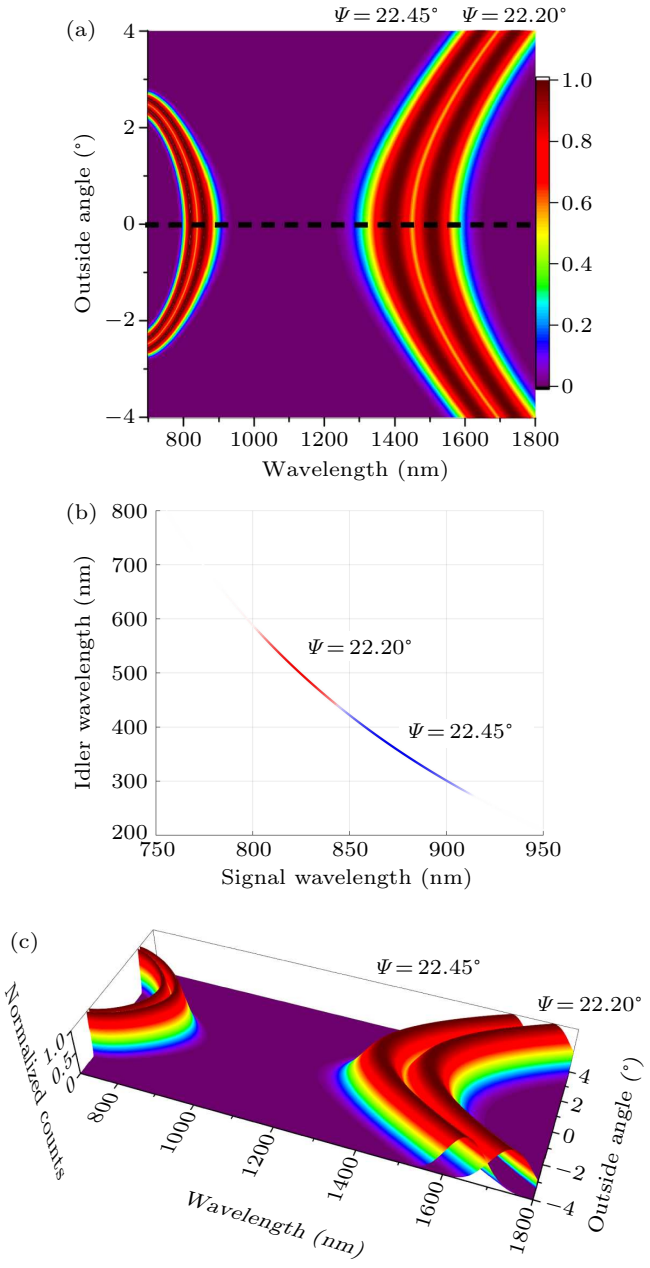


Fig. 3. Spatial distribution of the PDC photons versus wavelength for Ψ as 22.20° and 22.45°. (a) Top view. (b) Joint spectral distribution. (c) Three-dimensional view.

corresponding to the maximum counts are $\lambda_s = 880$ nm and $\lambda_i = 1390$ nm, and the bandwidths are $\Delta\lambda_s \simeq 148$ nm and $\Delta\lambda_i \simeq 410$ nm, respectively.

Considering the quantum efficiency of the SPD varies slightly over such a broad spectral range of more than 100 nm and even up to 400 nm, it is reasonable that the measured bandwidths are somewhat narrower than theoretical values. Moreover, for $\Psi = 22.20°$ or 22.45°, the experimental spectral curves agree well with the calculated ones in terms of peak position, shape, and trend, which confirms that the theoretical model is validly describes the complete spectral distribution of photon pairs generated in widely nondegenerate PDC.

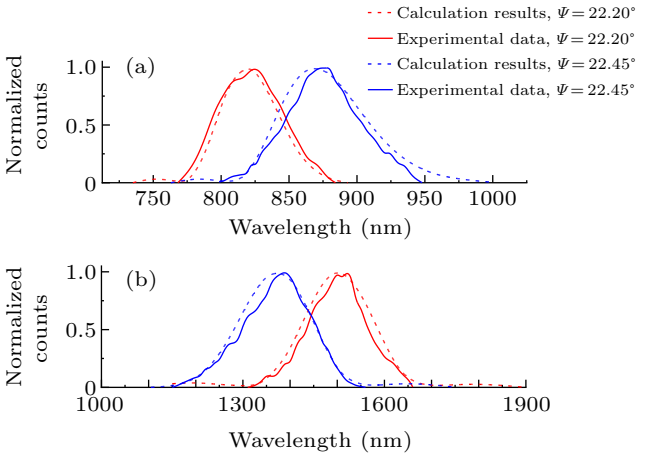


Fig. 4. Spectral distributions of (a) signal and (b) idler photons for $\Psi = 22.20°$ and 22.45°. Dashed line: theoretical result. Solid line: experimental result.

To reveal more interesting features, we calculate the PDC photon bandwidths at different peak wavelengths based on Eq. (3). Taking the signal photons as an example, theoretical results show that as the wavelength increases, the bandwidth gradually increases, which is clearly illustrated by the red dashed line in Fig. 5(a). The peak wavelengths range from 715–915 nm, covering a span of 200 nm, while the angle Ψ only changes from 21.4° to 22.6°.

Then we measure the bandwidths at these peak wavelengths one by one, and obtain the experimental results plotted as the solid line in Fig. 5(a). Comparing the calculated and measured data, one can find that they agree well with each other at shorter wavelengths. For longer wavelengths with wider bandwidth, due to the faster decrease of the SPD quantum efficiency, the measured bandwidths become narrower than the theoretical ones.

Regarding their spectral distinguishability, our analysis results show that when the peak wavelength of signal photons $\lambda_s < 915$ nm ($\Psi < 22.6°$), signal and idler photons are spectrally distinguishable as shown in Fig. 5(b). However, if λ_s continues to increase, they become partly spectrally indistinguishable (Fig. 5(c)), and it is no longer possible to clearly determine the bandwidths of signal or idler photons anymore. When $\lambda_s = \lambda_i = 1064$ nm, they are completely spectrally indistinguishable (Fig. 5(d)), and their bandwidths reach a maximum of approximately $\Delta\lambda_s = \Delta\lambda_i \simeq 500$ nm.

Finally, we analyze the photon number distribution during the whole spectrum range, and prepare heralded Fock states for near-infrared quantum key distribution. Using a PNR-SPD with a resolution of at least 10 photons (Fig. 6(a)), we measure in detail the photon number distributions at different wavelengths, calculate the average photons number, and compare it with the spectral distribution. The results are partially plotted in Fig. 6(b), from which we can observe that the average number of signal photons (red line) decreases similarly to the spectral distribution (blue line) on both sides of the peak wavelength. However, the average number of photons decreases slower than the spectral intensity measured by photon counting.

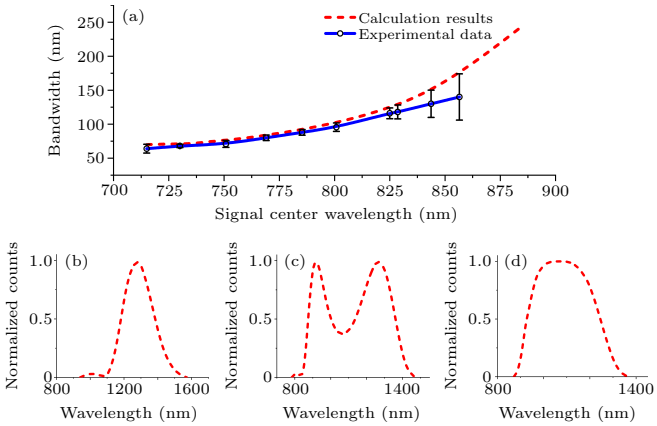


Fig. 5. (a) Bandwidths of the PDC spectrum versus signal center wavelengths λ_s. (b)–(d) Spectrum shapes of entangled photons and their spectral distinguishability, signal and idler photons are (b) distinguishable, (c) partially indistinguishable, and (d) fullly indistinguishable.

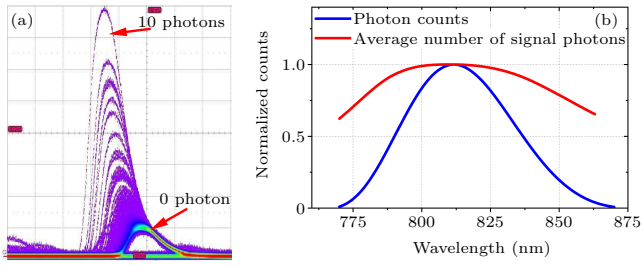


Fig. 6. (a) Output waveform of the PNR-SPD measured by a high-speed oscilloscope. (b) Spectral photon counts (blue line) and average number of signal photons (red line) as functions of wavelength.

4. Generation of heralded Fock states

Since the signal photons are entangled with the idler photons, we can use the signal photons as triggers to herald the near-infrared idler photons.[26] In the experiment, we add a multichannel analyzer after the PNR-SPD to select the required Fock states with photon numbers from 0 to 10. To increase the PDC efficiency, we choose another BBO crystal with a length three times longer than that of the former

one. Setting the pump laser power at 400 mW, we measure the generated Fock states and obtain their distribution as shown in Fig. 7, where one can find that the 5-photon Fock state has the maximum probability. After statistical analysis, we obtain the accurate distribution and illustrate it in Fig. 8, which shows that 5-photon Fock state has a probability close to 20%. The whole distribution deviates from a standard Poisson curve and approximately follows a quasi-Poisson distribution. Since the produced Fock states are carried by near-infrared photons in the fiber optical communication waveband, they can be directly applied to quantum key distribution in an optical fiber network.

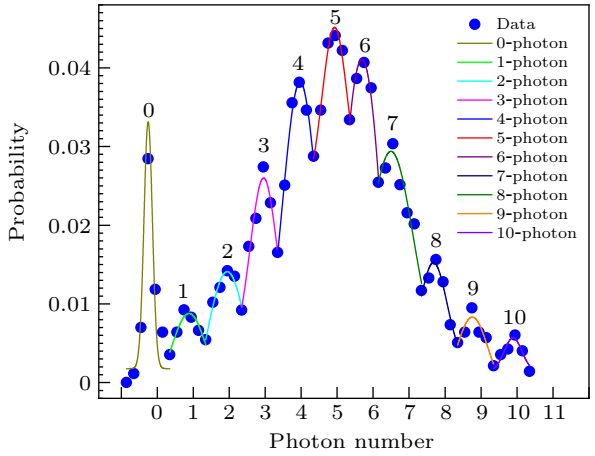


Fig. 7. Experimental results of heralded Fock states with 0 to 10 photons for near-infrared optical quantum communication.

To further determine the type of photon number distribution across the entire spectral range, we count and record the photon number by the PNR-SPD. For wavelengths at 770 nm, 790 nm, 810 nm, 835 nm, and 865 nm, the measured count rates we obtain are 60 cps, 150 cps, 330 cps, 150 cps, and 60 cps, respectively, while the dark counts are approximately 10 cps. After data processing based on Eq. (4), we obtain the photon number distributions shown in Fig. 9. Further analysis verifies that, for a wavelength of 810 nm near the peak, photon numbers obey nearly a quasi-Poisson distribution, while for wavelengths of 790 nm and 835 nm in the middle range, a multi-thermal distribution is the best. However, for 770 nm and 865 nm far away from the peak, a thermal distribution is better than others.

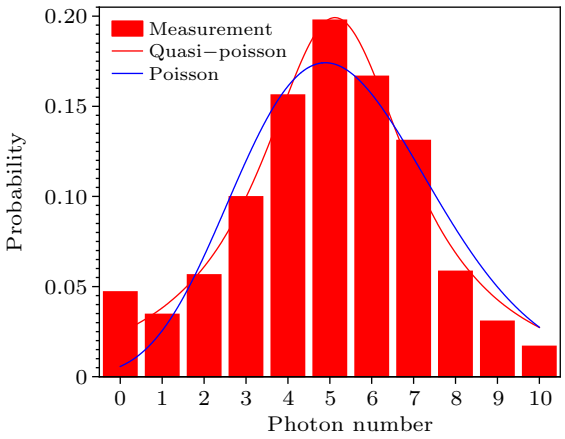


Fig. 8. Statistical photon-number distribution of generared Fock states.

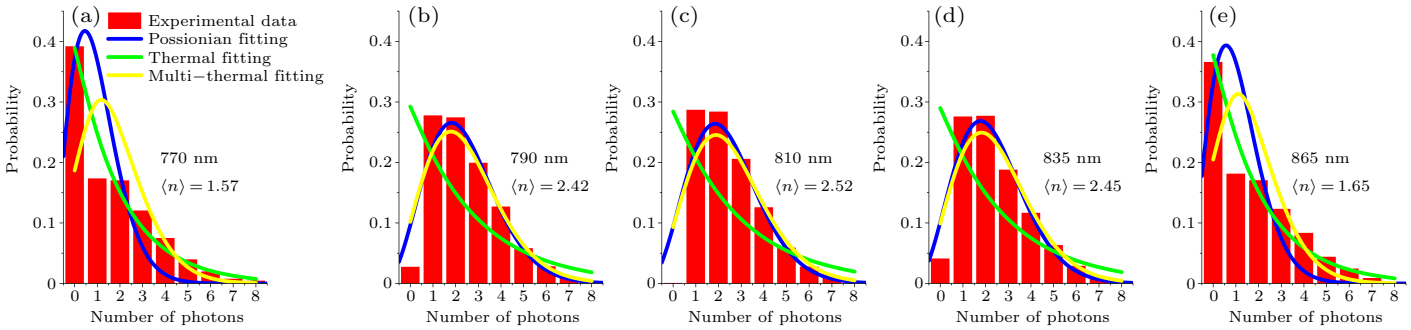


Fig. 9. Photon number distributions at different spectral wavelengths: (a) 770 nm, (b) 790 nm, (c) 810 nm, (d) 835 nm, and (e) 865 nm.

5. Conclusion

In summary, a convenient model is presented to describe the spatial-spectral distribution of PDC photon pairs, and successfully demonstrated experimentally by a 532-nm pumped PDC in a BBO crystal. Measured spectral curves of both signal and idler photons agree well with the theoretical results over the whole spectrum range. We further reveal the spectral distinguishability and bandwidth features, in our experiment, when the signal peak wavelength is less than 915 nm ($\Psi < 22.6°$), the photon pairs are spectrally distinguishable and their bandwidths can be determined accurately. When signal wavelength increases further, they become partly spectrally indistinguishable and no clear bandwidths can be obtained. Especially, when the signal wavelength reaches 1064 nm, they are completely spectrally indistinguishable with maximum bandwidths of approximately 500 nm. As signal wavelength increases, the idler bandwidth also broadens along with the signal's although its wavelength becomes shorter.

By employing PNR-SPDs, we demonstrate that the average photon number decreases much more slowly than the spectral intensity as the wavelength moves away from the peak, and

the photon numbers obey nearly a quasi-Poisson distribution around the peak, then multi-thermal distribution in the middle, finally the thermal distribution near the spectrum boundaries. Eventually, we use the signal photons as triggers to prepare heralded Fock states in near-infrared idler photons, and achieve Fock states with up to 10 photons.

Acknowledgment

Project supported by the National Natural Science Foundation of China (Grant No. 62075010).

References

[1] Pan J, Chen Z, Lu C, Weinfurter H, Zeilinger A and Zukowski M 2012 *Rev. Mod. Phys.* **84** 777
[2] Domeneguetti R, Stefszky M, Herrmann H and Silberhorn C 2023 *Opt. Lett.* **48** 2999
[3] Dirmeier T, Tiedau J, Khan I, Ansari V and Müller C 2020 *Opt. Express* **28** 30784
[4] Seifoory H, Vernon Z, Mahler D, Menotti M, Zhang Y and Sipe J 2022 *Phys. Rev. A* **105** 033524
[5] Seifoory H, Doutre S, Dignam M and Sipe J 2017 *J. Opt. Soc. Am. B* **34** 1587
[6] Perna A, Ortega E, Gräfe M and Steinlechner F 2022 *Appl. Phys. Lett.* **120** 074001
[7] Li B, Xie Y, Li Z, Weng C, Li C, Yin H and Chen Z 2021 *Opt. Lett.* **46** 5529
[8] Geng J, Fan-Yuan G, Wang S, Zhang Q, Chen W, Yin Z, He D, Guo G and Han Z 2021 *Opt. Lett.* **46** 6099
[9] Zhang J N, Zhang T Y, Duan J C, Gong Y X and Zhu S N 2024 *Chin. Phys. B* **33** 110301
[10] Chen Y H, Jiang Z and He G Q 2023 *Chin. Phys. B* **32** 090306
[11] Morris P, Aspden R, Bell J, Boyd R and Padgett 2015 *Nat. Commun.* **6** 5913
[12] Knill E, Laflamme R and Milburn G 2001 *Nature* **409** 46
[13] Kalashnikov D, Paterova A, Kulik S and Krivitsky L 2016 *Nat. Photonics* **10** 98
[14] Vallés A, Jiménez G, Salazar-Serrano L and Torres J 2018 *Phys. Rev. A* **97** 023824
[15] Paterova A, Yang H, Toa Z and Krivitsky L 2020 *Appl. Phys. Lett.* **117** 054004
[16] Pearce E, Phillips C, Oulton R and Clark A 2020 *Appl. Phys. Lett.* **117** 054002
[17] Tian Y, Cai W H, Yang Z X, Chen F, Jin R B and Zhou Q 2022 *Acta Phys. Sin.* **71** 054201 (in Chinese)
[18] Grice W, U'Ren A and Walmsley I 2001 *Phys. Rev. A* **64** 063815
[19] Kim Y and Grice W 2005 *Opt. Lett.* **30** 908
[20] Jin R B, Cai W H, Ding C, Mei F, Deng G W, Shimizu R and Zhou Q 2020 *Quantum Engineering* **2** e38
[21] Kuzucu O, Wong F, Kurimura S and Tovstonog S 2008 *Phys. Rev. Lett.* **101** 153602
[22] Lemos G, Borish V, Cole G, Ramelow S, Lapkiewicz R and Zeilinger A 2014 *Nature* **512** 409
[23] Scully M and Zubairy M 1997 *Quantum Optics* (Cambridge: Cambridge University Press)
[24] Boyd R 2008 *Nonlinear Optics* 3rd edn (San Diego: Academic Press)
[25] Liao T, Wang B C and Li Z Y 2020 *Opt. Commun.* **477** 126352
[26] Brańczyk A M, Ralph T C, Helwig W and Silberhorn C 2010 *New J. Phys.* **12** 063001